Biochimica et Biophysica Acta 1794 (2009) 297–308

Contents lists available at ScienceDirect

Biochimica et Biophysica Acta

journal homepage: www.elsevier.com/locate/bbapap

The 1.4 Å crystal structure of the large and cold-active *Vibrio* sp. alkaline phosphatase

Ronny Helland [a], Renate Lie Larsen [a], Bjarni Ásgeirsson [b,*]

[a] The Norwegian Structural Biology Centre, Department of Chemistry, University of Tromsø, N-9037 Tromsø, Norway
[b] Science Institute, Department of Biochemistry, University of Iceland, Dunhaga 3, IS-107 Reykjavik, Iceland

ARTICLE INFO

Article history:
Received 13 August 2008
Received in revised form 21 September 2008
Accepted 23 September 2008
Available online 15 October 2008

Keywords:
Cold-adaptation
Metalloenzyme
Dimer
Psychrophilic bacteria
Crystallography

ABSTRACT

Alkaline phosphatase (AP) from the cold-adapted *Vibrio* strain G15-21 is among the AP variants with the highest known k_{cat} value. Here the structure of the enzyme at 1.4 Å resolution is reported and compared to APs from *E. coli*, human placenta, shrimp and the Antarctic bacterium strain TAB5. The *Vibrio* AP is a dimer although its monomers are without the long N-terminal helix that embraces the other subunit in many other APs. The long insertion loop, previously noted as a special feature of the *Vibrio* AP, serves a similar function. The surface does not have the high negative charge density as observed in shrimp AP, but a positively charged patch is observed around the active site that may be favourable for substrate binding. The dimer interface has a similar number of non-covalent interactions as other APs and the "crown"-domain is the largest observed in known APs. Part of it slopes over the catalytic site suggesting that the substrates may be small molecules. The catalytic serines are refined with multiple conformations in both monomers. One of the ligands to the catalytic zinc ion in binding site M1 is directly connected to the crown-domain and is closest to the dimer interface. Subtle movements in metal ligands may help in the release of the product and/or facilitate prior dephosphorylation of the covalent intermediate. Intersubunit interactions may be a major factor for promoting active site geometries that lead to the high catalytic activity of *Vibrio* AP at low temperatures.

1. Introduction

The removal or transfer of phosphoryl groups is an important function in cellular metabolism and regulation. Enzymes have evolved along several lines to perform this function, despite the apparent simplicity of the reaction [1]. There are several classes of phosphatases depending on the presence or absence of metal ion cofactors such as zinc, magnesium, or iron. Some phosphatases must be under regulation at various levels and therefore have structural features allowing specific interactions with selected partners. Other phosphatases seem to be rather non-specific both in terms of substrate specificity and role. The family of alkaline phosphatases (APs) is widespread in nature and includes mostly members of the latter type. However, the failure of assigning a role to many of them may be due to lack of insight rather than the true state of affairs. Humans carry four isozymes depending on tissue distribution. A tissue-non-specific variant is expressed in many tissues and plays, for example, a role in bone mineralization [2]. Corresponding AP is found in lower vertebrates such as shrimp and fish. The isozymes have different thermal stabilities and respond differently to inhibitors. Thus, structural changes within the AP family take each member along a different evolutionary road depending on selective pressures from the environment, or for that matter, lack of selective pressures [3,4]. APs derive their name from the basic pH optimum of catalysis (k_{cat}), which is above pH 10 for enzymes from animals, but closer to pH 9 for bacterial variants [5–7]. In both cases, the optimum is somewhat removed from physiological pH. However, the vertebrate enzymes can achieve much higher catalytic rates (k_{cat}) than APs from mesophilic bacteria [8] which compensates for the effect of working at more than two pH-units below their optimum conditions. In fact, they display 20–30 fold higher catalytic activity than the reference AP from *E. coli* (ECAP) and yet the active-site structure is remarkably similar. It is clear, that this family of enzymes offers great opportunity to gain insight into fine-tuning of enzyme function through subtle differences.

Our interest in the AP from a cold-water *Vibrio* strain (VAP) has centred on its cold-adaptation. Previous biochemical studies have shown that APs with enhanced k_{cat} values exist in several organisms adapted to low temperature [6,7,9,10]. Two crystal structures have been solved for cold-active APs [11,12], in addition to wild-type and many mutants of ECAP [13], and the human PLAP isozyme [14]. These enzymes have remarkably dissimilar structural details but the core active-site structure is highly conserved. The bacterial APs span a spectrum in size, from a short polypeptide version found in the Antarctic bacterium strain TAB5 [10], through the medium-sized ECAP that has similar polymer chain length to mammalian variants, and culminating in the longest polypeptide version found in a North Atlantic *Vibrio* strain under study here. The size distribution variability and possible differences in oligomeric state of APs is most clearly seen

* Corresponding author. Tel.: +354 525 4800; fax: +354 525 89 11.
E-mail address: bjarni@raunvis.hi.is (B. Ásgeirsson).

1570-9639/$ – see front matter © 2008 Elsevier B.V. All rights reserved.
doi:10.1016/j.bbapap.2008.09.020

in the *Vibrio* genus, where, for example, five predicted AP genes are found in *V. vulnificus YJ016* (Q7MIW5, Q8DB10, Q8DBM0, Q8DDZ2, Q8D865). All give transcripts corresponding to the longest AP version similar to VAP. In contrast, the *V. cholera* AP gene remained unidentified until recently, even despite elucidation of the full genomic sequence. A gene quite different to other known AP genes was confirmed to produce the previously studied AP activity after cloning, sequencing, and protein expression. [15]. In fact, the *V. cholerae* AP sequence did not show homology with *Vibrio* G15-21 AP (VAP) [15,16], leading to the conclusion that AP from *V. cholera* was a unique enzyme differing greatly even from APs of closely related bacteria [15]. *V. cholerae* contains one of the earliest putative example of an active monomeric AP [17] but the more recent study [15] did not address the question of whether the original report of a monomeric active form was correct. In addition, the first cold-active AP studied was apparently monomeric [18]. Our interest in solving the crystal structure of the *Vibrio* AP (VAP) was partly to provide an answer to the question if this enzyme was also monomeric, since the shrimp AP (SAP) was reported to be active both as a monomer and a dimer [6]. The sequencing of the VAP polypeptide had suggested that a long insert loop might act as a surrogate second subunit [16]. At that time, it was the only long-chain representative in the data banks, and still is the only representative for which biochemical data is available [7]. A Swiss-Prot/TrEMBL search now reveals very similar sequences in several species, often obtained in large-scale sequencing projects, including *V. splendidus* (A3UWZ7), *V. harveyi* (A6AR48), *V. campbellii* (A8T5A5), *V. parahaemolyticus* (Q87MR7), *V. alginolyticus* (Q1VEG3), and *V. vulnificus* (Q7MIW5), but generally neither expression of these enzymes has been confirmed nor have their properties been studied.

The reaction mechanism of APs was first described in relation with the original ECAP structure [13] and more recently expanded based on further structural information [19]. The reaction mechanism of other APs has been formulated with reference to the structure of ECAP. The active site is characterized by three metal ions that all take part in the reaction pathway, in addition to a nucleophilic serine residue and an arginine that binds the negative charges of the phosphorous-oxygens. Sequence alignments between bacterial and mammalian variants show 25–30% identity but the structure around the active site is remarkably similar and conserved in terms of amino acid residues. Thus, only residues D153, T155, and K328 are different when comparing ECAP with mammalian and other bacterial APs. Furthermore, overall structural features are very similar with a central beta-sheet running through the dimeric structure with helices packed on either site. Most notable differences involve insertions and deletions, including the so-called “crown-domain”. The crown-domain notation was introduced with the PLAP structure [14]. Cold-adapted APs are of particular interest for being the catalysts with highest known k_{cat} values in this structural family [10,20,21]. Loops in the crown-domain create catalytically important conformational differences [22], allowing mammalian APs to be inhibited in a non-competitive manner by several amino acids and small peptides. One additional point of interest relating to the structure of APs is potential collaboration between subunits. This seems to depend on metal-site saturation. If metals are lacking, each monomer is dependent on the other for stability and catalytic performance. When fully metalated, the mammalian APs are non-cooperative allosteric enzymes (i.e. subunits independent, but each has regulatory subsites) [23]. Subunit interactions are influenced quite markedly by the N-terminal microenvironment, both in ECAP and mammalian APs [24], but that part is lacking in the VAP under study here.

A direct comparison of the refined ECAP structures with and without phosphate revealed a strong correlation between the occupancy of the third metal-binding site and the conformation of the S102 nucleophile [19]. The best conformation for nucleophilic attack by S102 in ECAP requires a magnesium ion in the third metal binding site. The other two metal sites are normally occupied by zinc. However, APs from organisms such as *Thermotoga maritima* and *Bacillus subtilis* require cobalt for maximal activity and function poorly with zinc and magnesium [25]. The amino acid residues that bind the two zinc atoms are conserved in all known APs, whereas there is some flexibility in which residues bind the third (magnesium) ion. This affects activity greatly, as numerous mutagenesis studies have shown [8,20,26]. ECAP has an aspartate (D153) where most other APs have a histidine. Histidine may increase the affinity of the third metal site for zinc and underlie stimulating effect of magnesium seen with many APs due to displacement of zinc from the third site. It also explains easy formation of triple zinc variants, for example in the crystal of SAP [11]. Furthermore, metal ion specificity is altered when the variable metal coordinating residues in ECAP are changed to the equivalent residues in mammalian APs (D153H and K328H). VAP has H116 (equivalent to D153 in ECAP) and W274 (equivalent to K328 in ECAP) and shares this with both TAP and APs from some more thermophilic organisms. It has been proposed that the H153/W328 (ECAP numbering) combination of residues selected for cobalt rather than zinc [27]. In fact, ECAP can effectively use cobalt instead of the zinc and magnesium when mutated to contain W328. We have recently analyzed metal content of wild-type VAP samples and only found zinc and magnesium, but no cobalt. VAP was very dependent on magnesium in buffers for maintenance of full activity, even at low temperature, suggesting loose association of the metal with the enzyme [20]. The X-ray structure was expected to give further information on this point.

The rate limiting step in the reaction mechanism of ECAP at alkaline pH is the release of product, i.e. non-covalently bound phosphate [5]. This conclusion has been carried over to describe reaction mechanism of all APs. However, caution should be levelled toward the possibility that the rate limiting step may be transferred to an earlier step in the pathway, such as the initial hydrolysis of the phosphoryl ester substrate or hydrolysis of the covalent phosphoryl–serine intermediate. Mutants have been made that show transfer of the rate determining step. An example is the K328C mutation in ECAP [28]. Furthermore, K328A and K328H ECAP mutants had much higher transphosphorylating than hydrolytic activity. This could not be explained purely by greater ease in releasing phosphate from the active site, but may be due to transfer of the slowest step to the hydrolysis of the covalently bound phosphoryl–enzyme complex [29]. As previously mentioned, APs of vertebrate origin have a histidine in position equivalent to ECAP K328, whereas VAP and a few other variants have a tryptophan.

Our aim with the present paper is to describe the structure of VAP and review the features that may relate to its high catalytic rate and cold-adaptation. Several AP crystal structures have been obtained in recent years with some distinct features. In addition to the original ECAP structure at 2.0 Å showing two zinc ions and one magnesium ion in the active site [13], the structures of the PLAP at 1.8 Å [14], SAP at 1.9 Å [11], and TAP at 1.95 Å [12] followed. Given the very high activity of the VAP variant, and the known sequence differences in the active site that partly create this enhanced activity [20], we were interested in cataloguing the structural features implicated in catalysis and compare with the rather rich background of the other structural relatives.

2. Materials and methods

2.1. Crystallization, data collection and refinement of VAP

Recombinant expression of VAP is described elsewhere [20] and protein purification was essentially as described previously [7]. Briefly, an initial affinity chromatography step on an L-histidyldiazobenzylphosphonic acid column was performed where the enzyme was eluted by adding 0.1 M potassium phosphate to the

Table 1
Data collection and refinement statistics

	Peak	Remote
Data collection		
Diffraction limit (Å)	2.0	1.4
Wavelength (Å)	1.2827	0.9184
Unit cell parameters (Å^3)		
a-axis (Å)	118.19	118.24
b-axis (Å)	165.92	165.98
c-axis (Å)	57.48	57.48
Space group	$P2_12_12$	$P2_12_12$
Total no. of reflections	945418 (58126)	883174 (46374)
No. of unique reflections	74311 (8728)	205938 (21811)
Completeness (%)	96.4 (80.1)	92.9 (68.8)
Anomalous completeness (%)	96.4 (79.8)	84.0 (44.4)
$I/\sigma(I)$	13.9 (13.2)	17.8 (10.1)
Mean ($\langle I\rangle$/sd(I))	50.1 (29.8)	30.4 (10.9)
R_{merge} (%)	4.1 (4.9)	2.7 (7.4)
Multiplicity	12.7 (6.7)	4.3 (2.1)
Wilson B (Å^2)	9.15	8.04
Outer shell resolution (Å)	2.11–2.00	1.48-1.40
Experimental phasing		
Phasing power	2.98	na
R_{Cullis}	0.44	na
Figure of merit	0.53	na
Refinement		
R-factor (%)	na	15.54
R_{free} (%)	na	16.65
Average *B* factors (Å^2)	na	8.05
No. protein atoms	na	8060
No. solvent molecules		
Zn^{2+}	na	4
Mg^{2+}	na	2
SO_4^{2-}	na	11
Ethylene glycol	na	3
Water	na	847
R.m.s. deviations		
Bond lengths (Å)	na	0.007
Bond angles (°)	na	1.177
Diffraction-component precision indicator		0.054
Ramachandran plot (%)		
Most favoured	na	91.7
Additionally allowed	na	8.3
Generously allowed	na	0
Disallowed	na	0

Outer shell values are given in parenthesis.
na: not available.

eluant. This was followed by a MonoQ anion exchange chromatography where the enzyme eluted at 0.15 M in a 0–0.7 M NaCl gradient. The columns were run with buffer containing 20 mM Tris, 10 mM $MgSO_4$, at pH 8.0, with 15% (v/v) ethylene glycol added in the MonoQ step to facilitate storage in frozen form. The protein was concentrated to 8 mg ml^{-1} and ethylene glycol concentration was reduced to 5% (v/v) prior to crystallization. Crystals of VAP suitable for X-ray diffraction studies were obtained by the hanging drop vapour diffusion method from reservoir solution containing 0.2 M Li_2SO_4, 0.1 M Tris pH 7.75, 23% PEG 3350 and 3% v/v ethylene glycol at 4 C temperature. X-ray data were collected at BL14.1 at Bessy. Data (Table 1) were processed in XDS [30], SCALA and TRUNCATE of the CCP4 program suite [31]. The crystal structure was solved using the single anomalous dispersion (SAD) technique on X-ray data collected to 2.0 Å on the K edge (1.2827 Å) of the catalytic zinc ions, and higher resolution data to 1.4 Å were collected on the same crystal at a remote wavelength (0.9184 Å). SHELXD [32] was used to identify four heavy atom sites which were further refined with SHARP [33]. The phases were improved by solvent flattening using SOLOMON [34]. Automatic tracing of the polypeptide chains, using the peak data, was carried out with ARP/wARP [35]. Subsequent improvement of the model was made using the data collected on the remote wavelength by manual refitting of side chains using O [36] based on sigmaA-weighted 2mFo-DFc and mFo-DFc electron density maps. Refinement was carried out in Refmac5 [37] of the CCP4 suite (Table 1).

Programs for structural comparison and analysis included the CCP4 suite, the DaliLite server (http://www.ebi.ac.uk/DaliLite/) [38] and the Secondary Structure Matching (SSM) server (http://www.ebi.ac.uk/msd-srv/ssm/ [39]). Selection of PDB entries for structural comparison was based on best hits from SSM and the nature of the ions in the active sites. Inserts and deletions were defined as regions which do, or do not, superimpose on VAP in the structural alignment using the DaliLite server. Estimation of intramolecular hydrogen bonds was carried out using HBPLUS [40] with a 3.4 Å distance criteria and default donor-acceptor angles of 90°. Analysis of the dimer interface included the use of the Protein interfaces, surfaces and assemblies service, PISA, at European Bioinformatics Institute (http://www.ebi.ac.uk/msd-srv/prot_int/pistart.html) [41]. Calculation of electrostatic surface potential was done using Delphi [42] with atomic partial charges from the AMBER molecular simulation program [43]. Illustrations were prepared in PyMOL (DeLano Scientific (http://pymol.sourceforge.net/)), with the exception of the structural alignment which was generated at the ESPript server (http://espript.ibcp.fr/ESPript/ESPript/) [44].

3. Results

3.1. Overall structure

Rod-like crystals up to 0.6×0.2×0.2 mm^3 grew from PEG3350, lithium sulphate, Tris pH 7.75 and ethylene glycol after three to four weeks. The crystal structure of VAP was determined to 2.0 Å using the single anomalous dispersion (SAD) technique on data collected 10 eV above the Zn K edge (1.2827 Å). Higher resolution data to 1.4 Å were collected on the same crystal at a remote wavelength (0.9184 Å). Data collection and refinement statistics are listed in Table 1. SHELXD [32] and SHARP [33] located four heavy atom sites, and using the experimental phases to 2.0 Å, ARP/wARP [35] could build 930 residues. Phase extension to 1.4 Å allowed auto-building of 980 of the 1004 residues in the VAP dimer. The final structure is refined to crystallographic *R*-factor of 15.54% and R_{free} of 16.65% and includes two VAP monomers (Fig. 1) containing two zinc and one magnesium

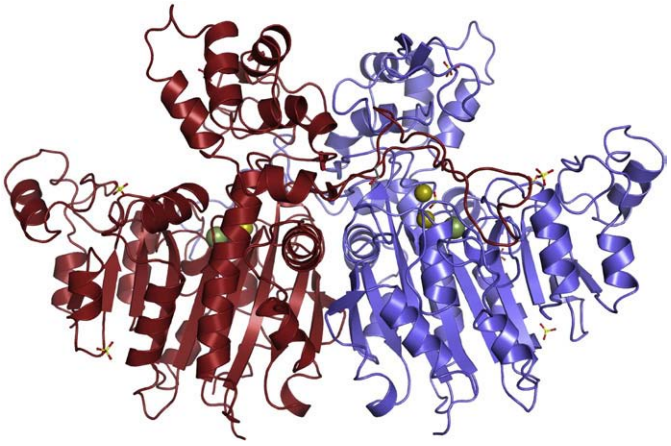

Fig. 1. Ribbon representation of VAP, where molecule A is coloured blue and molecule B is red. The conformation of unique insert II of the B molecule extending along the surface of molecule A is clearly visible. The "crown"-domain is located on the top of the figure and the catalytic zinc and magnesium ions located in the active site are represented as gold and green spheres, respectively. Sulphates and ethylene glycol are represented as ball-and-stick models.

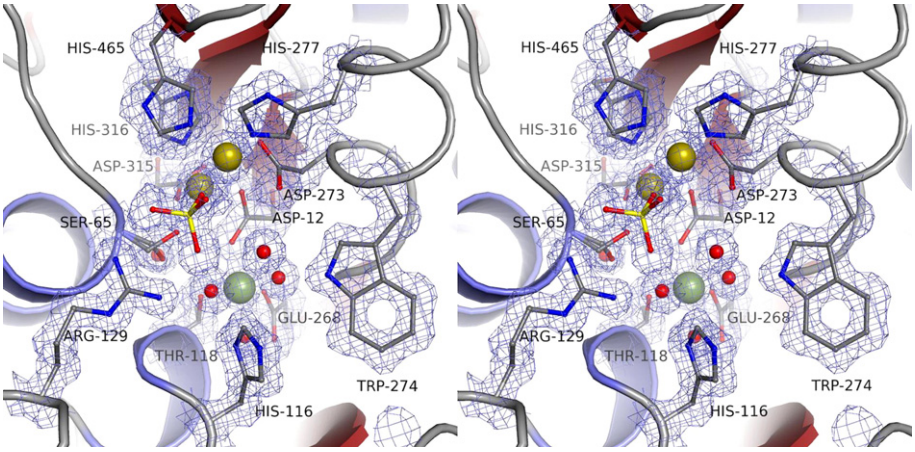

Fig. 2. Stereo-plot illustrating the electron density of the VAP active site, including the catalytic zinc (gold spheres) and magnesium (green sphere) ions, along with the sulphate (red and yellow ball-and-stick). Residues involved in metal coordination are also illustrated as ball-and-stick models whereas three water molecules are illustrated as red spheres. The catalytically important Ser65 is refined in two conformations. Zn1 is in front.

per monomer, eleven sulphates (six in MolA and five in MolB) and three ethylene glycol molecules (two in MolA and one in MolB). The electron density is generally well defined for all 1004 residues. The location of the zinc ions was verified by calculating the anomalous difference maps using data collected at the Zn K edge. The magnesium ion was identified using the sigma weighted mFo-DFc difference electron density and coordination and distances to neighbouring atoms [45]. Sulphate, or possibly phosphate trapped during expression or purification, is bound in the active site between the catalytically active S65, D12, H316, H465, R129, and the two zinc ions (Fig. 2). The two monomers superimpose on each other with a root mean square deviation (RMSD) value of 0.68 Å for all atoms. The largest RMSD differences (Fig. 3) observed for side chains are generally due to different conformations. The largest RMSD in the main chain is for residues 233–242. These form a loop connecting one of the outside helices to a short helix on top of the active site, an interesting area from a functional point of view. Residues 228–237 form a three-turn helix in MolB while only a two-turn helix is observed in MolA (residues 228–234). There are no significant close interactions to symmetry related neighbour molecules neither for MolA nor MolB forcing the monomers to adopt different conformations and explaining the difference. The electron density is well defined for the main chain for the 228–242 region in both molecules. The region consists, however, of a cluster of positively charged residues; three Lys and one Arg, which are not effectively stabilized by negatively charged residues or solvent molecules. Hence, the electron density for parts of the side chains is poorly defined. The difference in conformation of this region is likely to be responsible for the slightly higher RMSD values for the 164–173 region (insert I, see below) and the 339–343 region (insert II). The second region with large main chain RMSD values includes residues 370–387. Packing interactions are slightly different in MolA and MolB in this region. MolA is only in contact with N502 in a symmetry related molecule, while MolB contacts residues E93, K98, K101, A102, Q499, and N502.

3.2. Structural comparison to other APs

VAP, being the longest AP, was superimposed on Cα atoms of APs from ECAP, TAP, SAP, and PLAP (exemplified by PDB codes 1ed9, 2iuc, 1shq and 1zef, respectively), with RMSD values of 1.43–1.44 (ECAP; 322–324 residues), 1.30–1.40 (TAP; 312 residues), 1.38 (SAP; 334 residues) and 1.40 (PLAP; 327 residues) according to the SSM server (http://www.ebi.ac.uk/msd-srv/ssm/) [39]. The structural alignment is illustrated in Fig. 4.

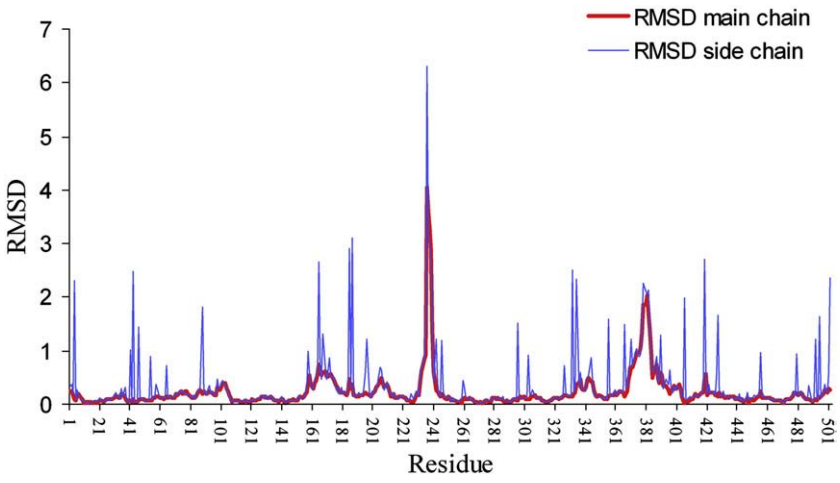

Fig. 3. RMS xyz displacement for superimposition of the two identical monomers of VAP (MolA on MolB).

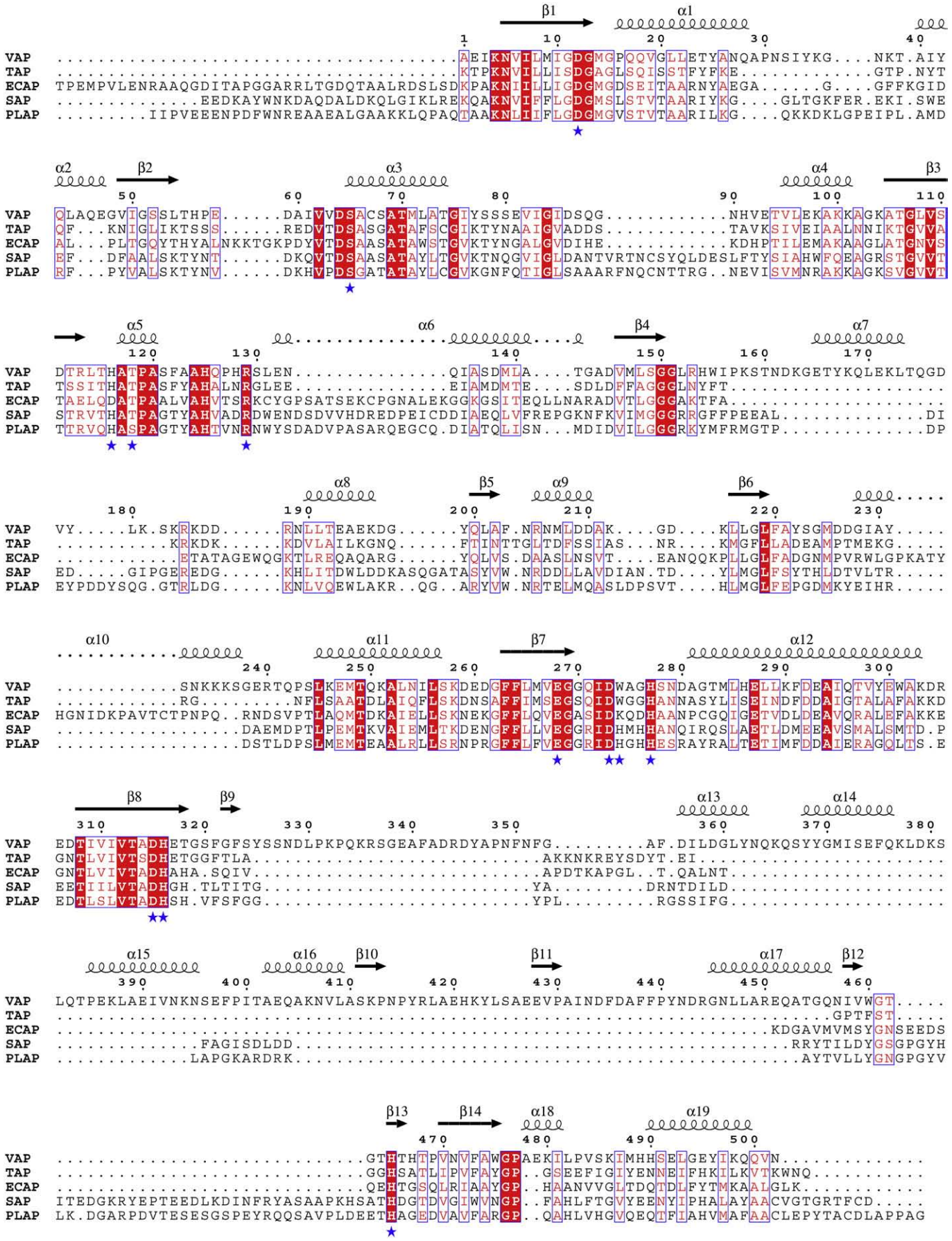

Fig. 4. Structural alignment generated by pairwise comparison of the structures of VAP, ECAP, TAP, SAP, and PLAP using the DaliLite structure comparison server (http://www.ebi.ac.uk/DaliLite/). The secondary structure of VAP (top) is illustrated. Blue stars indicate residues involved in metal binding or being involved in catalysis and specificity.

VAP is characterized by four inserts (Figs. 4 and 5a) having no counterpart in the homologous APs according to pairwise structural alignment using DaliLite (http://www.ebi.ac.uk/DaliLite/) [38]. These regions include residues 162–175 (insert I), 325–351 (insert II), 361–395 (insert III), and 405–450 (insert IV) by VAP numbering. Only insert I is not related to the crown-domain, known for being of different shapes and sizes in various APs. Regions absent in VAP according to the structural alignment (Fig. 5b) are generally due to different folding of the crown-domains. These regions include an insert of 14–15 residues in the VAP 133–134 region in SAP, PLAP, and ECAP, an insert of 10–20 residues in the VAP 89–90 region in SAP and PLAP, and a seventeen residue insert in the VAP 231–232 region in ECAP.

3.3. Insert I, residues 162–175

The thirteen residue insert, not being part of the crown-domain or the dimer interface, forms a three-turn helix (residues 158–173) in VAP. The other four homologous enzymes have loops in this region occupying different conformations. The loops in ECAP and TAP are shorter than in the eukaryotic APs. Attachment of the helix to the remaining enzyme is provided essentially through hydrophobic interactions, since the hydrogen bonds found in the helix region are primarily between main chain nitrogen and oxygen atoms of the loop itself (Supplementary Table 1).

3.4. Insert II, residues 325–351

This insert was initially believed to be located in the interface region, preventing formation of a biologically active dimer. The present structure shows that the twenty-six residue insert extends along the surface of the other monomer. The loop is characterized with relatively few intramolecular hydrogen bonds (twelve, Supplementary Table 1), where six are between main chain atoms. However, the loop, consisting of eight charged and nine non-polar residues, contributes significantly to the dimer stabilization by forming eleven intermolecular hydrogen bonds. Omitting this insert in calculation of buried water accessible surface area (ASA) in the dimer interface reduces the interface area from 4271 Å^2 to 2627 Å^2 (about 38%) per monomer (Supplementary Table 2).

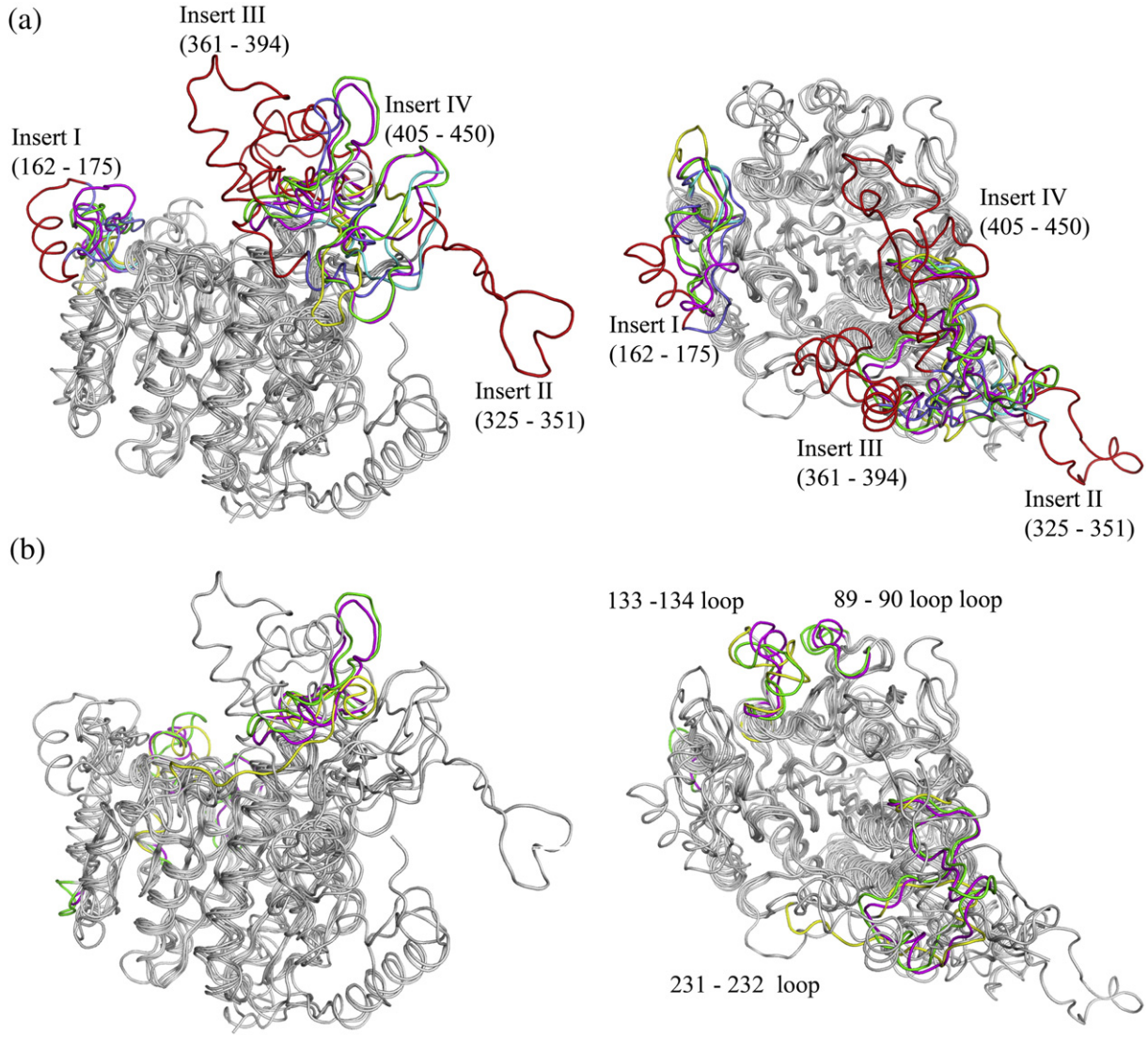

Fig. 5. Superimposition of VAP (red), TAP (cyan, PDB 2iuc), ECAP (yellow, PDB 1ed9) SAP (green, PDB 1shq), and PLAP (magenta, PDB 1zef). (a) Loop regions including the unique VAP regions colour coded red. Loops of the other APs in the same spatial regions are coloured to illustrate differences. (b) Regions with deletions in VAP are colour coded as described above.

3.5. Insert III, residues 361–394

The thirty-four residue insert folds into two helices (residues 368–376 and 385–395), separated by a loop including a three-residue 3_{10} turn. About 62% of the 45 hydrogen bonds formed by this loop are between main chain atoms, and similar to insert I, few include residues not being part of the loop itself. Although the loop is part of the crown-domain it is not part of the dimer interface region but rather extends on the other side over the active site crevasse.

3.6. Insert IV, residues 405–450

The forty-six residue insert consists mostly of loop structure containing two helices at the start and the end of the insert (residues 402–409 and 445–456) and two short strands (residues 411–413 and 428–430), forming an antiparallel sheet. More than half of the hydrogen bonds of this insert are, similar to the other inserts, between main chain atoms (Supplementary Table 2). The loop is involved in one of the two intermolecular salt-bridges D434 (MolA)–R450 (MolB), resulting in two of the four intermolecular salt bridges for the dimer. Omitting residues 405–450 from the calculation of buried ASA reduces the interface area from 4271 Å^2 to 3217 Å^2, about 24%, per monomer.

3.7. The active site

The active site of VAP consists of two zinc and one magnesium ions (Fig. 2). The Zn^{2+} ion at the M1 site is hexa-coordinated in a distorted octahedral arrangement by D273 (bidentate), H277, H465, and two oxygen atoms from Sul610 (or possibly a phosphate ion). The zinc ion at the M2 site is penta-coordinated by D12, S65, D315, H316, and one oxygen of Sul610. The Mg^{2+} ion at the M3 site is octahedrally hexa-coordinated by D12, T118, E268, and three waters. The residues involved in the first sphere of metal binding are conserved in the APs compared in this study, with the exception of residues around the M3 binding site. In the VAP H116 position, ECAP has an Asp while there are His in the other enzymes, and in the VAP T118 position PLAP has Ser while the other enzymes have Thr. Lastly, the residue at the VAP W274 position is also Trp in TAP, but Lys in ECAP, and His in SAP and PLAP. The conformation of the conserved metal ligands is similar in all five enzymes and differences in metal-ligand distances are generally less than 0.3 Å (Supplementary Table 3). Small displacements could be due to different ligands within the active site of the

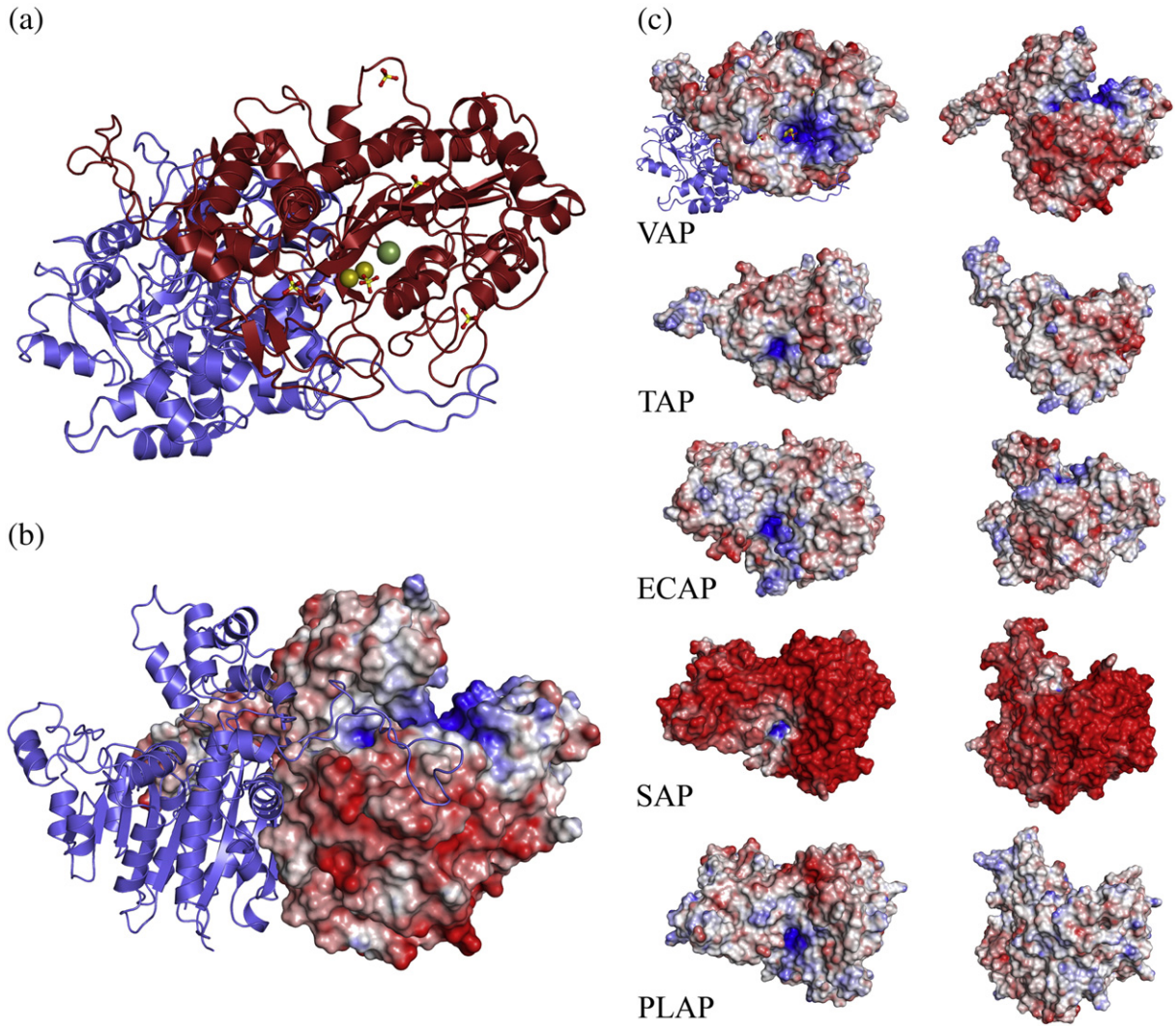

Fig. 6. (a) Ribbon presentation of VAP looking into the active site. (b) Standard view of VAP illustrating one monomer as ribbon, and the second with electrostatic surface potential. (c) Electrostatic surface potentials of VAP, TAP, ECAP, SAP and PLAP. The left view has the orientation of (a) and the right view the orientation of (b). The electrostatic surface potentials are contoured from −10 (red) to 10 (blue) kT/q.

crystals; namely sulphate in VAP and SAP, phosphite in PLAP and in TAP, and H_2O in ECAP. Sulphate in VAP is in a position to form interactions to both zinc ions and a bidentate interaction to R129 (ECAP R166). SAP has been solved with both sulphate and phosphate (PDB 1shq and 1shn, respectively) in the active site. Both anions occupy positions similar to sulphate in VAP, but interestingly, SAP R162 occupies different conformations in the two structures and the side chain is rotated away when the anion is sulphate. The phosphor-atom included in the TAP structure coincides with position of the sulphur-atom in the VAP structure, and R148 in TAP occupies the same position as R129 in VAP. Two of the oxygen atoms of phosphite in PLAP form bidentate interaction to R166. The nucleophilic S65 is refined in two conformations in VAP.

Tyr325 from the VAP B-subunit extends into the A-subunit substrate binding site with the hydroxyl group 4.69 Å from Zn at the M1 position. All the other APs, except ECAP, have a tyrosine residue at an equivalent position, although this cannot be seen from the structural alignment (Fig. 4): TAP; Y325 (B-subunit), 5.94 Å away from Zn1, SAP; Y366 (B-subunit), 5.64 Å from Zn1, PLAP; Y367 (symmetry related molecule), 5.43 Å from Zn1. In addition, VAP possesses a second tyrosine, Y44 from the A-subunit, where the hydroxyl group is 5.99 Å from Zn1 (A-subunit) and 2.67 Å from the hydroxyl of the B-subunit Y325.

The catalytic efficiency of an enzyme will depend on the substrate's accessibility to the active site. The large inserts in VAP are located close to the rim of the depression forming the catalytic site in most APs, such that the VAP catalytic site becomes relatively deeply buried in a crevice running between inserts III and IV on one side and the wing domain on the other (Fig. 1, Fig. 6). This crevice also contains three sulphate ions in addition to the sulphate coordinating the catalytic zinc ions, and one of them stabilizes the interaction between inserts III and IV. The somewhat narrow entrance to the active site appears to be partly compensated for by a relatively large positive potential which may attract the negatively charged phosphate of a substrate into the catalytic site (Fig. 6). The electrostatic attraction between opposite charges has on several occasions been reported to be central for the catalytic efficiency of enzymes from cold-adapted species (for review, see i.e. [46,47]). This positive potential in VAP is considerably larger than in the other APs, but it is difficult from the figure to estimate the role of the electrostatic potential to the cold-adaptation features of VAP.

3.8. The interface

Inserts II and IV contribute significantly to the dimer formation of VAP. Dimerization involves 115 residues and buries 4271 $Å^2$ of water accessible surface area (ASA) per monomer, or 19.7% of the total ASA (Supplementary Table 2). This is of the same order as the other APs, generally with 21–22% of the total ASA buried, but considerably more than in the cold-adapted TAP, with 1835 $Å^2$ or 14.1% of the total ASA buried. The small interface in TAP is attributed to the small (as visualized in Fig. 6) crown-domain together with the lack of an N-terminal helix as in PLAP and SAP or a corresponding large N-terminal loop as in ECAP [12]. VAP also lacks the N-terminal helix, but the stabilizing effects of the helix seem to be compensated for by insert II. Removing N-terminal amino acids prior to VAP position 1 (Fig. 4) in ECAP, PLAP, and SAP, and insert II in VAP before interface analysis yields a buried ASA of 2627–2839 $Å^2$ for VAP, PLAP, and SAP, and 2200 $Å^2$ for ECAP. Removing insert IV in VAP, further reduces the buried ASA to 2100 $Å^2$, hence, being of the same order as the other bacterial APs (ECAP and TAP). There is no apparent trend in the percentage of charged residues in the interface regions of the five APs, with the exception of SAP being considerably more negatively charged overall and no ionic interactions being present in TAP over the dimer interface. Interestingly, the percentage of non-polar residues in the VAP interface (40%) approaches that of PLAP (45%), while the fractions in the other three APs are in the range 30–34% (Supplementary Table 2).

4. Discussion

4.1. General

We are now in a position to compare the extra large version VAP to two other cold-active variants, one very short version from the Antarctic bacterium strain TAB5 (TAP), the other medium sized from Northern shrimp (SAP). In addition, two AP variants from mesophilic organisms (ECAP and PLAP) have previously been solved structurally that are both medium sized in length. The quality of the structure obtained here for VAP is at a very good resolution of 1.4 Å with no part of the polypeptide unclear or excluded due to, for example, movements of loops. It confirms that the VAP is a dimer. It is also shown here for the first time how the insert in the sequence (insert II; 325–351), that in particular characterizes VAP, attaches the monomers together, thus taking the role of the N-terminal subunit connections in ECAP, SAP, and PLAP. This part of the polypeptide has inherently a remarkably little secondary structure as predicted by computational analysis (data not shown).

4.2. Metal coordination and water in the active site

The structure confirms previous analysis [20] that the metal ions in the active site are two zinc ions and one magnesium. Some of the AP structures have contained three zinc ions in the active sites [11,14]. Still other structures have contained additional metal binding sites, such as for calcium and magnesium, proposed to be of functional importance [4,12]. No additional metal binding-sites were found in VAP as in some other APs, but several binding sites for sulphate and ethylene glycol originating from the solvents were observed that point to potential regulatory interactions with other molecules.

ECAP exhibits maximal activity when zinc fills the M1 and M2 sites and magnesium is present in site M3 [25], but APs can work with other metal ions. In fact, an AP variant from the thermophilic *T. maritima* has been suggested to be preferentially ligated with cobalt due the fact that K328 (ECAP numbering) is a tryptophan and D153 is a histidine [25,48]. This is the same metal ligands as in the VAP under study here. Any generalization about the preference of the M3 sites for other ions than magnesium if tryptophan and histidine occupy the positions in question is refuted by the present results and our previous direct atomic absorption measurements [20].

All three metal ions take part in the catalysis and the magnesium ion is also important for stability. The latter abstracts the proton from the nucleophilic serine through generation of a metal-bound hydroxide ion. This mechanism is assumed to be a general one. All-zinc containing enzymes have a lower activity but can be reactivated with magnesium for optimal activity at alkaline pH [49]. Addition of zinc to many APs is inhibitory. The different effects may be due to sub-optimal coordination of the magnesium-bound hydroxide ion in the initial nucleophilic attack by different ions [50]. In SAP, zinc in M3 can be replaced by magnesium by extensive dialysis, and this triggers H149 to adopt a conformation in which it does not coordinate the metal ion [11], but instead superimposes with the corresponding histidines in PLAP, TAP, and now also VAP, which all contain magnesium in M3.

The backbone positions of the VAP metal ligands fit very closely to the structure of ECAP and the other APs. The M1 and M2 ligands are all in a very close alignment through the backbone, and side chains also superimpose well. The two M3 ligands that are identical in all APs also superimpose, but the two residues that differ between various APs are slightly out of alignment. The side chain of W274 (ECAP K328) in the second variable position lies in the same plane as the corresponding lysine in ECAP. The Trp rings in VAP (W274) and TAP (W260) are in the

same plane as the corresponding histidine in PLAP (H317) and the nitrogen atoms superimpose well. In SAP, H316 differs from PLAP H317 by a 45° rotation of the imidazole ring through the Cβ-Cγ bond. The plane of the imidazole ring of VAP H116 in the first variable position is rotated about 55° relative to the plane of the carboxyl group of ECAP D153. The imidazoles of H135 in TAP and H153 in PLAP occupy conformations almost identical to VAP H116, while H149 in SAP is rotated about 50° through the Cβ-Cγ bond in the structure containing magnesium at M3 (PDB 1shn). Despite slightly different conformations of the side chains, all distances between the ligand and the magnesium ion are of the same order of around 4 Å (Supplementary Table 3). The mutation H135D in TAP [26] (D153 in ECAP) resulted in a more stable but less active enzyme. The TAP H135 had two possible conformations with magnesium in M3 which could not be distinguished [12]. The published model was built with reference to PLAP with Nε2 pointing toward R148 (VAP R129, ECAP R166) but it could also take part in the M3 water shell analogous to the function of the Asp153 in ECAP, a structure suggested by the authors to be more likely.

At alkaline pH, the release of product is the slowest step in ECAP [5], where K328 stabilizes phosphate binding through a water mediated interaction. Weakening of this interaction increases product release dramatically [29]. The single K328H mutant had a lower binding constant for phosphate that produced a higher catalytic rate, whereas affinity for substrate was little changed. Differences in metal coordination and strength of interaction with phosphate can explain higher activity in the ECAP cobalt variant of the D153H/K328W mutant compared with wild-type. VAP and TAP have a tryptophan in the position corresponding to K328 that would suggest a similar mechanism for activity enhancement, whereas SAP and PLAP have histidine in this position. In the D153H/K328H ECAP mutant, the hydrolysis of the covalent intermediate becomes partially rate-limiting because product release is very fast [29]. We do not know if this is the case for the VAP, but changing the two residues to the ones corresponding to ECAP had dramatic effect on activity as well as stability [20]. The contention that rate of product release is rate liming in all APs should be approached with caution as universal, especially since ECAP is rather the exception when it comes to residue choice in the two positions referred to above.

The AP structures have water molecules at conserved positions in the otherwise empty active sites. This is also seen in VAP, where three waters are located around the magnesium ion in the same positions as similar waters in the other structures. These are involved in the catalytic function and their exact location might influence the proficiency of catalysis.

4.3. Conformation of key residues

Motional freedom of the residues involved in catalysis is closely linked with enzyme function such as binding of substrates and release of products. Such considerations gain added weight when one tries to discover the subtle differences that make enzyme variants particularly cold-active, as is the case for VAP. In VAP, the nucleophilic S65 (ECAP S102) is on a helix that superimposes very closely onto a corresponding ECAP helix. The active site Ser65 was refined in two different conformations, illustrating a flexible nature of the side chain. This coincides with S84 in TAP which had several possible positions. The most common position (χ=60°) placed the serine oxygen atom in roughly the same conformation as in the ECAP and PLAP structures with transition state mimics, and within the coordination sphere of the M2 ion.

Arg129 is another active site residue involved in the initial binding of substrate and the release of product as mutational studies on ECAP (R166) have shown. The arginine's conformational position is known to be different in the AP crystal structures. Two positions were possible in SAP; “docked” (PDB 1shn) and “non-docked” (PDB 1shq and 1k7h). The presence of substrate or inhibitor was deemed a likely prerequisite for it to adopt the docked position in SAP [11,51], and the authors concluded that non-docked R162 might facilitate the release of product and be a factor in cold-active properties. The conformation of VAP R129 superimposes well on the corresponding residues in ECAP, PLAP (PDB 1zef) and the “docked” conformation in SAP. Interestingly, R162 in SAP adopts the “docked” conformation when phosphate is present at the active site and Zn at M3, but not in the presence of sulphate and magnesium in M3. The anion-free structure having Zn in M3 (1k7h) adopts the “non-docked” conformation. Thus, the conformation of R162 in SAP appears to be linked to the nature of the anion at the active site, and not necessarily the metal at M3. R166 in PLAP also adopts the “docked” conformation with phosphite at the active site. Based on these observations, the hypothesis that the anion bridging the two zinc ions in VAP (interpreted as Sul610) could indeed be a phosphate trapped in expression or purification is highly likely.

4.4. Surface characteristics and access to the active site

The interactions of APs with various substrates and inhibitors have revealed some preferences that relate back to the active site structure as well as general surface characteristics. A very negatively charged surface has been observed in some cold-adapted enzymes, including SAP, indicating that it may help catalysis through directing substrate approach to the positive charge around the active site [11]. A similar negative electrostatic surface of the cold-adapted VAP and TAP is not observed. Instead their surfaces resemble more ECAP and PLAP. VAP has a slightly larger positive potential area surrounding the active site (Fig. 6), possibly being involved in attracting the negatively charged substrate into the active site at reduced temperatures. A special feature of VAP is how inserts III and IV shield the active site. The “overhang” may regulate interactions of VAP with substrates in some as yet unknown manner through specific binding. No other substrates apart from p-nitrophenol phosphate and activity stain have been used to assay VAP activity, so it cannot be stated yet that it is non-specific. Recently, we have discovered that VAP is inhibited by various amino acids like vertebrate APs [23] indicating that it can accommodate small organic molecules in a specific manner (Ásgeirsson, unpublished).

4.5. Structural and functional features of the dimeric interface

One of the main revelations brought to light in this study is the dimeric nature of VAP. Biochemical evidence that earlier pointed toward the existence of an active monomeric form included size-exclusion chromatography, activity staining in native electrophoresis gels [7], and attempts at cross-linking the monomers (unpublished work). Although most well characterized APs are dimers, there are still some contentious reports of active monomeric forms [17,18]. In light of the VAP structure presented here, this would seem increasingly unlikely.

The dimer interface is a determinant of stability and how well metals bind. There is also close synergy between the monomers in various APs; they do not function independently of one another. Cooperation between subunits has been proposed for calf intestinal AP to facilitate the release of product in a half-of-sites model, involving communication over the interface [5,52]. From the earliest studies on ECAP, kinetic evidence was forwarded that implemented a conformation change as the rate-determining step in catalysis [53] presumably to assist in release of the non-covalently bound product, the phosphate ion. More recently, subunit communications have been discovered in PLAP where residues from one subunit become part of the active site in the second one [23]. A similar phenomenon is found in VAP, where Tyr325 from the B-subunit extends into the A-binding site. Closer inspection of the APs included here reveals that all, except ECAP, have a tyrosine from the second monomer in the active site of the first monomer.

Dissociation of the AP dimers by urea or guanidinium leads to inactivation [54–56]. The dimers in cold-adapted enzymes are held together by weaker interaction than in mesophilic variants which may explain part of their improved catalytic action through increased mobility [6,55]. Cooperativity in substrate hydrolysis, or the allosteric interactions suggested for some APs, would be affected by interactions at the interface that lies close to the two active sites. However, oligomerization appears in many cases to be driven by the need to increase stability rather than shape activity. Thus, cold-adapted enzymes might have weakened monomer interactions due to lack of evolutionary pressure to enhance temperature stability. The least extensive interface connections are seen in the smallest representative of the AP family, the cold-active TAP where the interface has fewer H-bonds than the ECAP interface and no salt bridges. However, the present results show very similar number of non-covalent interactions between monomers in VAP compared with much more heat-tolerant variants (Supplementary Table 2). In most APs, the N-terminal forms an extended loop or helix that embraces the other monomer creating increased stability. Examples include the ECAP, SAP, and PLAP. The TAP variant seems only to rely on the interface area, where the opposite main walls of the two monomers touch, although the first thirty residues, approximately, were missing from the structural data. The N-terminal region is not present in the VAP but instead it has a unique loop as part of the crown-domain (insert II) that seems to serve the same function. Proteolytic cleavage of the N-terminal end from ECAP resulted in rearrangement of secondary structures and change in tertiary and quaternary properties [57]. This unique arrangement in VAP may have some function in loosening the structure to improve activity.

4.6. Crown-domain

The "crown"-domain is the most conspicuous structure in APs due to its variable size and role as a connection between subunits. VAP has the most extensive crown of known APs and it must have a significant role in regulating monomer/dimer interactions. The crown area is noticeably larger in VAP compared with PLAP, the enzyme with the best defined role for this region. Similar to PLAP and SAP, a short antiparallel sheet is preserved there in VAP (Fig. 7). In PLAP, each crown-domain contributes three small beta strands (362–364, 391–395, and 423–425) to form a six-stranded double sheet layer with the other monomer [14]. In SAP, each crown-domain contains four small beta-strands (360–363, 377–380, 384–388, and 390–392) forming two adjacent hairpin motifs, where the 360–363 and 390–392 strands (strands 1 and 4) align with the 362–364 and 391–395 strands in PLAP, respectively, hence forming a four-stranded double sheet with the other monomer. The two strands conserved in PLAP and SAP are also found in VAP, but shorter (322–323 and 458–459), whereas the middle antiparallel unit in SAP has developed into the large intersubunit loop. Insert II occupies some of the same space as parts of the SAP hairpin strands 2 and 3, while on the opposite side of the crown-domain, inserts III (not visible in Fig. 7) and IV extend over the active site.

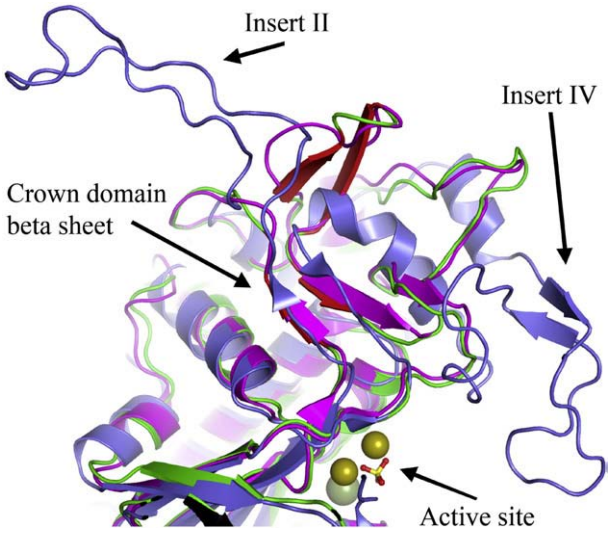

Fig. 7. Crown-domain of VAP (blue), SAP (green), and PLAP (magenta). The hairpin motif in SAP is coloured red. Zinc (gold spheres), magnesium (green sphere), and sulphate representing the active site are illustrated at the bottom of the figure.

A physiological role for the crown-domain has been shown in the mammalian APs. Most recently, a conservative replacement of valine by alanine in the crown-domain of the human tissue-non-specific AP (TNAP) was shown to cause defective mineralization in a prenatal form of hypophosphatasia [58]. This mutant showed a marked reduction in activity, with k_{cat}/K_m less than one-tenth that of the wild-type enzyme. It maintained the dimeric structure but was more susceptible to proteolysis, indicating a subtle distortion of the crown-domain. More specific conclusion were not possible, but residues in the crown-domain have in many cases direct effects on the enzymatic properties, in particular in relation to surface loops that differ conformationally in the various isozymes and modulate catalytic parameters in the presence of protein ligands [59]. In human PLAP, the allosteric regulation of activity within each subunit by binding of amino acids to the crown region is well documented [4]. Crown-domains attach to adjacent beta-strands in the central beta-sheet and may thus cause internal movement.

In VAP, as in other APs, one of the M1 Zn-ligands (VAP H465, ECAP H412) is located toward the end of the polypeptide chain. It follows immediately after the crown-domain and is closest to the interface of the ligands. The strand which it is part of forms a partial area of the interface. The main chain of H465 forms a hydrogen bond to the side chain of S324 at the start of insert II of the other monomer, and the H465 side chain is close to Y325 from the other monomer which extends into the active site. Movement in the crown-domain, or at the interface, might produce displacements in this part of the active site. Zn1 participates in the first phase of the reaction when the activated hydroxyl of the Ser102 (ECAP) attacks the phosphorous centre of the substrate by bridging an oxygen atom of the substrate and facilitating the departure of the alcohol leaving group [19]. The role of the Zn1 ion in the second phase of the reaction mechanism is proposed to be the lowering of the pKa of a coordinating water molecule to effectively form the nucleophilic hydroxide ion [19]. The magnesium-coordinated water molecule then reprotonates the nucleophilic serine, or may directly protonate the phosphate group, and, thus, facilitate the departure of the product [19]. Mobility of the active site arginine (ECAP R166, VAP R129) side chain may also facilitate the release of phosphate from the enzyme–product non-covalent complex, which is the slowest step for wild-type ECAP under alkaline conditions.

5. Conclusions

Several questions have been answered with the present result. Early reports on APs from an Antarctic bacteria species [18] or *Vibrio cholera* [17] maintained that they were monomeric. Initial characterization of the enzyme under study here pointed in the same direction. Since most other APs are inactive as monomers, it was suggested that the large insert in the sequence of VAP might form a surrogate second subunit by covering the dimerization area. The present study shows that the VAP can form dimers and that the extra inserts in residues add to the "crown" area to form an even larger additional part than observed in PLAP and SAP. There is an interesting twist, however, in the fact that the N-terminal region, a main stabilizer of dimer interactions in ECAP, PLAP, and SAP, is absent in VAP. Instead, a large part of the insert sequence located to the second half of the

polypeptide comes to play the same role on the opposite site of the structure.

Features that might be linked with cold-adaptation do not stand out clearly in the three structures now available. Cold-adaptation in SAP was largely traced to extensive negative potential on its surface that would facilitate interaction with the solvent through hydrogen bonding and directing substrates to the active site [11]. Similar tendencies in amino acid content have been observed in various cold-adapted enzymes; including fewer hydrophobic residues, higher percentage of polar residues, lower arginine content, and fewer prolines. In TAP, cold-adaptation was linked with more abundance of glycines, which would create backbone mobility, together with a reduction in prolines. Although this notion is not universally true, importance of glycine clusters has been shown in TAP by mutagenesis [60]. More recent studies using directed evolution indicate that cold-adaptation is mostly created by substitution located close to the active site [21]. Furthermore, global destabilization towards heating is not enough to improve k_{cat}; other structural constrains must also be fulfilled. It is interesting that the substitutions in TAP that gave less stability (S42G, S338T) occur naturally in VAP (G11, T446). In TAP, the k_{cat} values of these substitutions were, however, lower than wild-type. Another study involving directed evolution of ECAP showed that the introduction of only two mutations sufficed not only to provide a bacterial enzyme with high catalytic activity comparable with mammalian APs, but almost maintained its high original thermostability [61]. The effect was clearly associated with D330N that lies 12 Å from the centre of the catalytic pocket pointing toward the interface and next to the M1 ligand H331. It may be uniquely responsible for the acceleration of the release of product into the medium producing a two- to three-fold increase in activity. The double ECAP mutant D153G/D330N increased k_{cat} a further seven-fold, giving a bacterial enzyme as active as the mammalian APs. Structural analysis showed that the Asn and Asp side chains on residue 330 were fully superimposable. However, a covalent phosphoseryl intermediate was observed and some differences in the distance to the M2 zinc. Thus, the mutation made the covalent intermediate apparently more stable than the non-covalent one, probably due to acceleration of the phosphate release [61]. VAP has a glycine in the position corresponding to D330. It remains to be tested if this site can affect VAP catalysis by allowing some fine-tuning of distances within the active site. This could affect the stability of metal ion binding, and thus, strengthen interactions and/or the exact position of the phosphate containing groups the active site can accommodate.

Comparison of cold-adapted AP structural variants with mesophilic counterparts and mutagenesis experiments suggest that many subtle changes in structure can be brought into play to adjust the activity within each enzyme family. It is still difficult to pinpoint any general rules. In fact, the variability in size and surface characteristic within cold-adapted APs is somewhat remarkable. In the VAP structure, the most noticeable characteristic is the large crown-domain and long extension loops that connect monomers and cover the active site. These features may contribute to minimizing the structural inertia that cold-environments would favour. We can propose that the catalytic rate of VAP may be affected by the nature and positioning of the ligands to the third metal site carrying the magnesium. Movement of the active site serine that interacts with the hydroxide/water molecule bound to the magnesium seems plausible due to multiple positions in MolA and MolB, and movement of R129 that binds negative charges to the shallow crevice of the catalytic site as previoulsy mentioned is also likely involved. This may affect hydrolysis of the covalent enzyme-phosphate intermediate and/or release of non-covalently bound phosphate, since both steps are experimentally known to be rate determining in APs. A stronger positive electric field may attract substrate but may also retard product release, unless the negative charge is strongly subdued by salt ions such as sodium. Activity of VAP is actually strongly enhanced at NaCl concentrations from 0 to 300 mM (Ásgeirsson, unpublished results). The role of the positive field does not seem to affect substrate binding as indicated by the fact that K_m values of cold-active APs are generally relatively large. That fits the theory of a more flexible active site giving more extensively dynamic motions than in less active variants. Motion is linked with the mass of the domains that the enzymes carry. The VAP has a larger crown-domain than other known APs. If this mattered for enzyme-activity, VAP would be expected to have one of the highest k_{cat}. And it does.

Acknowledgments

Financial support from the Icelandic Research Fund is gratefully acknowledged as well as access to beam time at the Berliner Elektronenspeicherring (BESSY). This project was supported by The Norwegian Structural Biology Centre (NorStruct) which is financed by the national program in Functional Genomics (FUGE) under the Research Council of Norway. We thank Dr. Ellen Wang for setup of initial screens for crystallization conditions and Dr. Ed Hough and Prof. Arne Smalås in particular for support and encouragement.

Appendix A. Supplementary data

Supplementary data associated with this article can be found, in the online version, at doi:10.1016/j.bbapap.2008.09.020.

References

[1] J.B. Vincent, M.W. Crowder, B.A. Averill, Hydrolysis of phosphate monoesters — a biological problem with multiple chemical solutions, Trends Biochem. Sci. 17 (1992) 105–110.
[2] P.S. Henthorn, M. Raducha, K.N. Fedde, M.A. Lafferty, M.P. Whyte, Different missense mutations at the tissue-nonspecific alkaline phosphatase gene locus in autosomal recessively inherited forms of mild and severe hypophosphatasia, Proc. Natl. Acad. Sci. U. S. A. 89 (1992) 9924–9928.
[3] M.H. Le Du, J.L. Millan, Structural evidence of functional divergence in human alkaline phosphatases, J. Biol. Chem. 277 (2002) 49808–49814.
[4] P. Llinas, E.A. Stura, A. Menez, Z. Kiss, T. Stigbrand, J.L. Millan, M.H. Le Du, Structural studies of human placental alkaline phosphatase in complex with functional ligands, J. Mol. Biol. 350 (2005) 441–451.
[5] J.E. Coleman, Structure and mechanism of alkaline phosphatase, Ann. Rev. Biophys. Biomol. Struct. 21 (1992) 441–483.
[6] R.L. Olsen, K. Øverbø, B. Myrnes, Alkaline phosphatase from the hepatopancreas of shrimp (*Pandalus borealis*): a dimeric enzyme with catalytically active subunits, Comp. Biochem. Physiol. 99B (1991) 755–761.
[7] J.B. Hauksson, Ó.S. Andrésson, B. Ásgeirsson, Heat-labile bacterial alkaline phosphatase from a marine *Vibrio* sp. Enz. Microbial. Technol. 27 (2000) 66–73.
[8] J.E. Murphy, E.R. Kantrowitz, Why are mammalian alkaline phosphatases much more active than bacterial alkaline phosphatases? Molec. Microbiol. 12 (1994) 351–357.
[9] B. Ásgeirsson, R. Hartemink, J.F. Chlebowski, Alkaline phosphatase from Atlantic cod (*Gadus morhua*). Kinetic and structural properties which indicate adaptation to low temperatures, Comp. Biochem. Physiol. 110B (1995) 315–329.
[10] M. Rina, C. Pozidis, K. Mavromatis, M. Tzanodaskalaki, M. Kokkinidis, V. Bouriotis, Alkaline phosphatase from the Antarctic strain TAB5 properties and psychrophilic adaptations, Eur. J. Biochem. 267 (2000) 1230–1238.
[11] M. de Backer, S. McSweeney, H.B. Rasmussen, B.W. Riise, P. Lindley, E. Hough, The 1.9 Å crystal structure of heat-labile shrimp alkaline phosphatase, J. Mol. Biol. 318 (2002) 1265–1274.
[12] E. Wang, D. Koutsioulis, H.K. Leiros, O.A. Andersen, V. Bouriotis, E. Hough, P. Heikinheimo, Crystal structure of alkaline phosphatase from the Antarctic bacterium TAB5, J. Mol. Biol. 366 (2007) 1318–1331.
[13] E.E. Kim, H.W. Wyckoff, Reaction mechanism of alkaline phosphatase based on crystal structures, J. Mol. Biol. 218 (1991) 449–469.
[14] M.H. Le Du, T. Stigbrand, M.J. Taussig, A. Menez, E.A. Stura, Crystal structure of alkaline phosphatase from human placenta at 1.8 Å resolution. Implication for a substrate specificity, J. Biol. Chem. 276 (2001) 9158–9165.
[15] A. Majumdar, A. Ghatak, R.K. Ghosh, Identification of the gene for the monomeric alkaline phosphatase of *Vibrio cholerae* serogroup O1 strain, Gene 344 (2005) 251–258.
[16] B. Ásgeirsson, Ó.S. Andrésson, Primary structure of cold-adapted alkaline phosphatase from a *Vibrio* sp. as deduced from the nucleotide gene sequence, Biochim. Biophys. Acta 1549 (2001) 99–111.
[17] N.K. Roy, R.K. Ghosh, J. Das, Monomeric alkaline phosphatase of *Vibrio cholerae*, J. Bacteriol. 150 (1982) 1033–1039.
[18] H. Kobori, C.W. Sullivan, H. Shizuya, Heat-labile alkaline phosphatase from Antarctic bacteria: rapid 5′ end-labeling of nucleic acids, Proc. Natl. Acad. Sci. U. S. A. 81 (1984) 6691–6695.

[19] B. Stec, K.M. Holtz, E.R. Kantrowitz, A revised mechanism for the alkaline phosphatase reaction involving three metal ions, J. Mol. Biol. 299 (2000) 1303–1311.
[20] K. Gudjónsdóttir, B. Ásgeirsson, Effects of replacing active site residues in a cold-active alkaline phosphatase with those found in its mesophilic counterpart from *Escherichia coli*, FEBS J. 275 (2008) 117–127.
[21] D. Koutsioulis, E. Wang, M. Tzanodaskalaki, D. Nikiforaki, A. Deli, G. Feller, P. Heikinheimo, V. Bouriotis, Directed evolution on the cold adapted properties of TAB5 alkaline phosphatase, Protein Eng. Des. Sel. 21 (2008) 319–327.
[22] M.F. Hoylaerts, J.L. Millan, Site-directed mutagenesis and epitope-mapped monoclonal antibodies define a catalytically important conformational difference between human placental and germ cell alkaline phosphatase, Eur. J. Biochem. 202 (1991) 605–616.
[23] M.F. Hoylaerts, T. Manes, J.L. Millan, Mammalian alkaline phosphatases are allosteric enzymes, J. Biol. Chem. 272 (1997) 22781–22787.
[24] M.F. Hoylartes, L. Ding, S. Narisawa, S. Van kerckhoven, J.L. Millán, Mammalian alkaline phosphatase catalysis requires active site structure stabilization via the N-terminal amino acids micrenvironment, Biochemistry 45 (2006) 9756–9766.
[25] J. Wang, K.A. Stieglitz, E.R. Kantrowitz, Metal specificity is correlated with two crucial active site residues in *Escherichia coli* alkaline phosphatase, Biochemistry 44 (2005) 8378–8386.
[26] I. Tsigos, K. Mavromatis, M. Tzanodaskalaki, C. Pozidis, M. Kokkinidis, V. Bouriotis, Engineering the properties of a cold active enzyme through rational redesign of the active site, Eur. J. Biochem. 268 (2001) 5074–5080.
[27] C.L. Wojciechowski, E.R. Kantrowitz, Altering of the metal specificity of *Escherichia coli* alkaline phosphatase, J. Biol. Chem. 277 (2002) 50476–50481.
[28] L. Sun, D.C. Martin, E.R. Kantrowitz, Rate-determining step of *Escherichia coli* alkaline phosphatase altered by the removal of a positive charge at the active center, Biochemistry 38 (1999) 2842–2848.
[29] X. Xu, E.R. Kantrowitz, A water-mediated salt link in the catalytic site of *Escherichia-coli* alkaline phosphatase may influence activity, Biochemistry 30 (1991) 7789–7796.
[30] W. Kabsch, Automatic processing of rotation diffraction data from crystals of initially unknown symmetry and cell constants, J. Appl. Cryst. 26 (1993) 795–800.
[31] N. Collaborative Computational Project, The CCP4 suite: programs for protein crystallography, Acta Crystallogr. D Biol. Crystallogr. 50 (1994) 760–763.
[32] T.R. Schneider, G.M. Sheldrick, Substructure solution with SHELXD, Acta Crystallogr. D Biol. Crystallogr. 58 (2002) 1772–1779.
[33] E. De la Fortelle, G. Bricogne, Maximum-likelihood heavy-atom parameter refinement for the multiple isomorphous replacement and multiwavelength anomalous diffraction methods, Meth. Enzymol. 276 (1997) 472–494.
[34] J.P. Abrahams, A.G. Leslie, Methods used in the structure determination of bovine mitochondrial F1 ATPase, Acta Crystallogr. D Biol. Crystallogr. 52 (1996) 30–42.
[35] A. Perrakis, R. Morris, V.S. Lamzin, Automated protein model building combined with iterative structure refinement, Nat. Struct. Biol. 6 (1999) 458–463.
[36] T.A. Jones, J.Y. Zou, S.W. Cowan, Kjeldgaard, Improved methods for building protein models in electron density maps and the location of errors in these models, Acta Crystallogr. A 47 (Pt 2) (1991) 110–119.
[37] G.N. Murshudov, A.A. Vagin, E.J. Dodson, Refinement of macromolecular structures by the maximum-likelihood method, Acta Crystallogr. D Biol. Crystallogr. 53 (1997) 240–255.
[38] L. Holm, J. Park, DaliLite workbench for protein structure comparison, Bioinformatics 16 (2000) 566–567.
[39] E. Krissinel, K. Henrick, Secondary-structure matching (SSM), a new tool for fast protein structure alignment in three dimensions, Acta Crystallogr. D Biol. Crystallogr. 60 (2004) 2256–2268.
[40] I.K. Mcdonald, J.M. Thornton, Satisfying hydrogen-bonding potential in proteins, J. Mol. Biol. 238 (1994) 777–793.
[41] E. Krissinel, K. Henrick, Inference of macromolecular assemblies from crystalline state, J. Mol. Biol. 372 (2007) 774–797.
[42] W. Rocchia, E. Alexov, B. Honig, Extending the applicability of the nonlinear Poisson–Boltzmann equation: multiple dielectric constants and multivalent ions, J. Phys. Chem. B 105 (2001) 6507–6514.
[43] D.A. Case, T.E. Cheatham, T. Darden, H. Gohlke, R. Luo, K.M. Merz, A. Onufriev, C. Simmerling, B. Wang, R. Woods, The Amber biomolecular simulation programs, J. Computat. Chem. 26 (2005) 1668–1688.
[44] P. Gouet, E. Courcelle, D.I. Stuart, F. Metoz, ESPript: analysis of multiple sequence alignments in PostScript, Bioinformatics 15 (1999) 305–308.
[45] M.M. Harding, Small revisions to predicted distances around metal sites in proteins, Acta Crystallogr. D Biol. Crystallogr. 62 (2006) 678–682.
[46] G. Feller, C. Gerday, Psychrophilic enzymes: hot topics in cold adaptation, Nat. Rev. Microbiol. 1 (2003) 200–208.
[47] A.O. Smalås, H.-K. Schroder Leiros, V. Os, N.P. Willassen, Cold adapted enzymes, in: M.R. El-Gewely (Ed.), Biotechnol. Ann. Rev. 6, Elsevier, 2000, pp. 1–57.
[48] C.L. Wojciechowski, J.P. Cardia, E.R. Kantrowitz, Alkaline phosphatase from the hyperthermophilic bacterium *T. maritima* requires cobalt for activity, Protein Sci. 11 (2002) 903–911.
[49] W.F. Bosron, R.A. Anderson, M.C. Falk, F.S. Kennedy, B.L. Vallee, Effect of magnesium on the properties of zinc alkaline phosphatase, Biochemistry 16 (1977) 610–614.
[50] B. Stec, M.J. Hehir, C. Brennan, M. Nolte, E.R. Kantrowitz, Kinetic and X-ray structural studies of three mutant *E. coli* alkaline phosphatases — insights into the catalytic mechanism without the nucleophile Ser102, J. Mol. Biol. 277 (1998) 647–662.
[51] M.M.E. de Backer, S. McSweeney, P.F. Lindley, E. Hough, Ligand-binding and metal-exchange crystallographic studies on shrimp alkaline phosphatase, Acta Crystallograph. D Biol. Crystallogr. 60 (2004) 1555–1561.
[52] D. Chappelet-Tordo, M. Fosset, M. Iwatsubo, C. Gache, M. Lazdunski, Intestinal alkaline phosphatase. Catalytic properties and half of the sites reactivity, Biochemistry 13 (1974) 1788–1794.
[53] I. Hinberg, K.J. Laidler, The kinetics of reaction catalysed by alkaline phosphatase: the effects of added nucleophiles, Can. J. Biochem. 50 (1972) 1360–1368.
[54] M.C. Falk, J.L. Bethnu, B.L. Vallee, Formamide-induced dissociation and inactivation of *Escherichia coli* alkaline phosphatase. Metal-dependent reassociation and restoration of activity from isolated subunits. Biochemistry 21 (1982) 1473–1478.
[55] B. Ásgeirsson, J.B. Hauksson, G.H. Gunnarsson, Dissociation and unfolding of cold-active alkaline phosphatase from Atlantic cod in the presence of guanidinium chloride. Eur. J. Biochem. 267 (2000) 6403–6412.
[56] B. Ásgeirsson, K. Gudjónsdóttir, Reversible inactivation of alkaline phosphatase from Atlantic cod (*Gadus morhua*) in urea, Biochim. Biophys. Acta 1764 (2006) 190–198.
[57] R. Tyler-Cross, C.H. Roberts, J.F. Chlebowski, Proteolytic modification of *Escherichia coli* alkaline phosphatase, J. Biol. Chem. 264 (1989) 4523–4528.
[58] N. Numa, Y. Ishida, M. Nasu, M. Sohda, Y. Misumi, T. Noda, K. Oda, Molecular basis of perinatal hypophosphatasia with tissue-nonspecific alkaline phosphatase bearing a conservative replacement of valine by alanine at position 406. Structural importance of the crown domain, FEBS J. 275 (2008) 2727–2737.
[59] M. Bossi, M.F. Hoylaerts, J.L. Millan, Modifications in a flexible surface loop modulate the isozyme-specific properties of mammalian alkaline phosphatases, J. Biol. Chem. 268 (1993) 25409–25416.
[60] K. Mavromatis, I. Tsigos, M. Tzanodaskalaki, M. Kokkinidis, V. Bouriotis, Exploring the role of a glycine cluster in cold adaptation of an alkaline phosphatase, Eur. J. Biochem. 269 (2002) 2330–2335.
[61] B.H. Muller, C. Lamoure, M.H. Le Du, L. Cattolico, E. Lajeunesse, F. Lemaitre, A. Pearson, F. Ducancel, A. Menez, J.C. Boulain, Improving *Escherichia coli* alkaline phosphatase efficacy by additional mutations inside and outside the catalytic pocket, Chembiochem 2 (2001) 517–523.